

Excellence in Chemistry Research

Announcing our new flagship journal

- Gold Open Access
- Publishing charges waived
- Preprints welcome
- Edited by active scientists



Meet the Editors of *ChemistryEurope*



Luisa De Cola

Università degli Studi
di Milano Statale, Italy



Ive Hermans

University of
Wisconsin-Madison, USA



Ken Tanaka

Tokyo Institute of
Technology, Japan

Special
Collection

Enhanced Electrochemical Performance of NTP/C with Rutile TiO₂ Coating, as Anode Material for Sodium-Ion Batteries

Teja Stüwe,^[b] Daniel Werner,^[b] David Stock,^[c] Christoph W. Thurner,^[b] Alexander Thöny,^[b] Christoph Grießer,^[b] Thomas Loerting,^[b] and Engelbert Portenkirchner*^[a]

NaTi₂(PO₄)₃ (NTP) is known as a promising insertion-type anode material for aqueous and non-aqueous sodium-ion batteries (SIBs), due to its NASICON-type open 3D framework which makes a zero-strain insertion mechanism possible. NTP is considered to be an environmentally friendly, low-cost and high safety material. However, the electrochemical performance of NTP is limited due to its poor electrical conductivity. In this work a solvothermal synthesis method is used to synthesize NTP with a nanocube (NC) morphology. In a one-step synthesis rutile titanium dioxide (TiO₂) and carbon coating of NTP are achieved (NTP/C-RT), simultaneously, which significantly im-

proves the poor electrical conductivity of NTP. Additional rutile coating is used to further improve the electrochemical performance compared to simple carbon coating. Rate capabilities of 301 mAh/g are achieved for NTP/C-RT compared to 248 mAh/g for NTP/C at 0.1 C. That is, to the best of our knowledge, the highest gravimetric capacity reported for SIBs using NTP as anode material up to now. The results prove that NTP, which is itself already a promising anode material for SIBs, can be further enhanced with a combined approach of NC morphology, carbon and rutile coating, leading to superior capacities, higher than anywhere else reported in literature.

Introduction

Energy storage devices, like rechargeable batteries, are a key component towards an efficient and carbon-neutral electricity production in the future.^[1]

In the past decade lithium-ion batteries (LIBs) have been used for most battery-powered applications and have consequently dominated the battery market. LIBs demonstrate the highest energy density of current, state of the art rechargeable batteries. Nevertheless, in the past few years there have been concerns about shortage of lithium (Li) supply, high carbon footprint of Li production, toxicity of state-of-the-art cathode

materials and safety issues of flammable organic electrolytes employed in LIBs.^[2]

These concerns about LIBs have led to an increasing interest towards post-lithium type batteries. Among these, SIBs are an interesting candidate due to the natural abundance and low-cost of sodium. Furthermore, the progress in SIB research has been very fast and fostered by a similar Li and Na-ion chemistry.^[3] The possibility to use water-based electrolytes, which are cheaper, safer, ecologically friendly and easier to recycle than organic electrolytes, is another advantage over LIBs.^[4] The main challenge is the change in chemical bonding between the Na-ion and electrode material and the large size and higher mass of the Na-ion compared to the Li-ion which leads to a lower energy density and causes problems with intercalation/ deintercalation of Na-ions into the cathode and anode materials.^[5,6]

Owing to the fast development of SIB technology, many anode and cathode materials have already been investigated.^[7–10] On the cathode side, layered sodium transition-metal oxides, polyanion-based materials and Prussian-blue materials are among the most studied compounds.^[3,11,12] Anode materials include insertion type materials, like carbons and transition-metal oxides and phosphates, alloying and conversion reaction materials.^[11,13]

For aqueous rechargeable SIBs, even though a lot of research has been devoted into this field, there are still major challenges that have to be overcome before its successful commercialization.^[15]

Among many anode and cathode materials, which have been tested in aqueous systems, especially carbon-coated NaTi₂(PO₄)₃ has been proven to show great battery performance

[a] Dr. E. Portenkirchner
Department of Physical Chemistry
University of Innsbruck
Innrain 52C, 6020 Innsbruck (Austria)
E-mail: Engelbert.Portenkirchner@uibk.ac.at

[b] T. Stüwe, D. Werner, C. W. Thurner, A. Thöny, C. Grießer, Dr. T. Loerting
Department of Physical Chemistry
Leopold-Franzens-University Innsbruck
Innrain 52C, 6020 Innsbruck (Austria)

[c] D. Stock
Institute of Material Technology
Leopold-Franzens-University Innsbruck
Technikerstraße 13, 6020 Innsbruck (Austria)

Supporting information for this article is available on the WWW under <https://doi.org/10.1002/batt.202300228>

Part of Special Collection dedicated to Battery Research in Europe

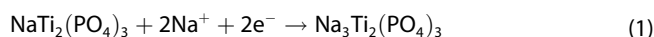
© 2023 The Authors. Batteries & Supercaps published by Wiley-VCH GmbH. This is an open access article under the terms of the Creative Commons Attribution License, which permits use, distribution and reproduction in any medium, provided the original work is properly cited.

characteristics. NTP is considered as promising insertion-type anode material for aqueous, as well as for non-aqueous SIBs.^[16]

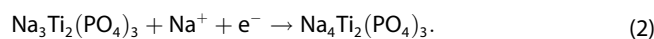
The sodium storage mechanism for rutile TiO₂ differs significantly from that of NTP. While NTP shows an insertion type mechanism during sodiation, rutile forms an active surface film composed of Na₂O₂. Little to no Na-ion intercalation is found in the bulk oxide. This surface film can grow during battery cycling leading to increased capacity retention.^[17,18]

The NASICON-type structure of NTP makes zero-strain Na-ion insertion possible, resulting in a high Na-ion conductivity.^[19] NTP has a relatively high theoretical capacity of 133 mAh/g.^[20,21] The NASICON-type 3D framework, shown in Figure 1(a), has a crystal structure containing isolated [TiO₆] octahedra and [PO₄] tetrahedra which are connected by corner-sharing oxygen atoms.^[22,23] This structure is characterized by large interstitial sites suitable for Na-ion intercalation and deintercalation with little lattice strain.^[24]

A typical cyclo-voltammogram (CV) of NTP is shown in Figure 1(b). NTP reacts with Na⁺ and electrons *via* a two-step mechanism. In the first step the reduction of Ti^{IV} to Ti^{III} occurs, described by the following Reaction (1):



In the second step Ti^{III} is further reduced to Ti^{II}, according to Reaction (2):^[25]



Many strategies have been developed to further enhance the electrochemical performance of NTP, which is mainly limited by its low electrical conductivity. Important enhancement strategies include synthesis of NTP nanoarchitectures, nanolayer coatings, adding carbonaceous materials or ion doping.^[26]

Nanostructures can improve the electrochemical performance significantly due to the shortening of the Na-ion diffusion distance. The type of nanostructure is thereby dependent on the synthesis method chosen. Another common way to enhance the poor electrical conductivity of NTP is material coating. By far the most applied strategy is carbon coating, which improves the electrical contact between particles. The coating can be achieved either in a one-step method or in a second step, after the NTP synthesis.^[21] The one step method of carbon coating can reduce the particle size as it inhibits crystal growth during sintering.^[27,28]

Other compounds like Al₂O₃, TiO₂ or SiO₂ have been used for nanolayer coating. The conventional method is atomic layer deposition.^[21,29]

In this work a facile solvothermal synthesis method is chosen to prepare uniformly and highly symmetrical nanocubes (NCs) coated with rutile in a one-step method (Figure 1e). In a

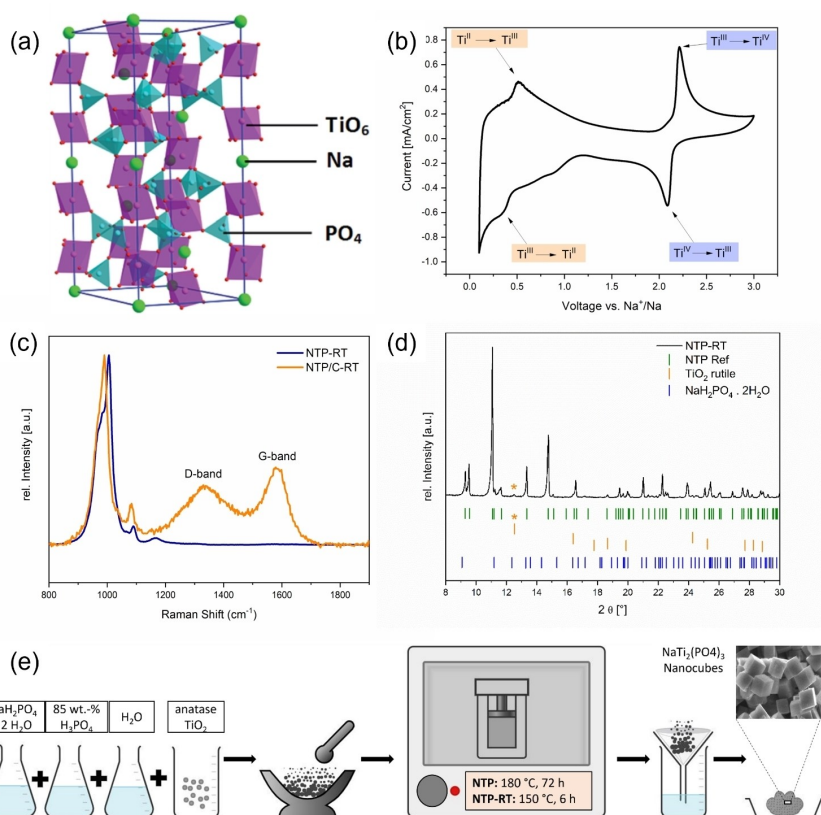


Figure 1. a) Crystal structure of the NASICON-type NTP,^[14] b) typical CV of NTP with the corresponding Ti redox processes at a scan rate of 0.1 mV/s, c) Raman spectra of NTP-RT and carbon-coated NTP/C-RT, d) powder XRD diffractogram of NTP with reference Bragg peak positions, e) schematic representation of the solvothermal synthesis method for NTP&NTP-RT.

second step additional carbon coating is applied. Carbon as well as rutile coating enhances the poor electrical conductivity of pristine NTP.

Results and Discussion

Figure 1(c) shows Raman spectra of NTP-RT and NTP/C-RT (Raman spectra of NTP and NTP/C can be found in the SI Figure S5a). Similar band shapes and band patterns can be observed between 800 and 1100 cm^{-1} for NTP as well as for NTP/C. Therefore, a similar NTP structure exists in both samples. All peaks (Supporting Information Figure S5a and c) were assigned to the corresponding bond vibrations and are listed in the Supporting Information Table S2.^[30] There are two broad bands in the carbon-coated sample at 1330 and 1579 cm^{-1} .

These two bands can be attributed to the D- and G-band of graphite.^[31] The relative intensity of D and G-bands were calculated to be 0.77. This indicates amorphous carbon and proves a successful carbon coating.^[32] The carbon content was determined by thermogravimetric analysis (TGA), see Supporting Information Figure S7.

Figure 1(d) shows the XRD powder pattern of NTP-RT (XRD pattern of NTP can be found in the Supporting Information Figure S4a).

The synthesized NTP-RT exhibits high purity for crystallites of relevant size, as all major Bragg peaks can be assigned to NTP. A Bragg peak, which can be attributed to rutile is identified at 2θ equal to 12.5° . Further characterization of the successful rutile coating is given in the Supporting Information Figures S4(b), S5(b) and S6(a,b). Figure 2(a) shows the morphology of NTP, which is characterized by uniformly, highly symmetrical and dispersed NCs. The NCs differ in size, with an average edge length of about 1 μm . The surface of the NTP NCs is smooth without any observable defects, suggesting a crystalline nature.

Similar to NTP, highly symmetrical NTP-RT NCs are visible in the SEM images shown in Figure 2(c). Compared to NTP, slightly more defects of the NCs surface can be seen. This observation

might be attributed to the synthesis method, as a lower reaction temperature (180 vs. 150 $^\circ\text{C}$) and a shorter reaction time (72 vs. 6 h) has been chosen for the synthesis of NTP-RT compared to NTP. Consequently, the SEM images suggest that NTP NCs need a longer reaction time and/ or higher temperatures to properly form without defects. The increased number of surface defects, however, does not have a negative impact on the electrochemical performance, considering that NTP-RT shows superior results over NTP. It has yet to be investigated to what extent the increased number of surface defects contributes to the enhanced electrochemical performance of NTP-RT.

Figure 2(b and d) shows SEM images of symmetrically and uniformly dispersed NTP/C and NTP/C-RT NCs, respectively. Compared to NTP and NTP-RT, NTP/C as well as NTP/C-RT NCs are characterized by a significantly higher number of defects in combination with small particles on the surface. Alternation of the NTP NCs could occur during the carbon-coating procedure where the NTP sample are heated to 600 $^\circ\text{C}$ for 4 h. However, the change of the NCs surface does not have a negative impact on the electrochemical performance.

Comparing the rutile coated samples to NTP and NTP/C in Figure 3(c,d), we see a significant increase in sodiation and desodiation capacities and more distinct voltage plateaus. The superior performance of the rutile coated anode materials agrees well with previous observations in the CV measurements (Figure 3a,b). NTP and NTP-RT exhibit lower capacities and more sloping voltage-capacity curves due to the larger polarization and lower electrical conductivity. The desodiation plateaus in the non carbon-coated samples are at more positive voltages than in the carbon-coated electrodes which can also be explained by the larger polarization.

The rate performance of NTP, NTP-RT, NTP/C and NTP/C-RT is investigated in Figure 4. Sodiation and desodiation cycles of NTP/C-RT are shown in Figure 4(c) at different C-rates of 0.1, 0.5 and 1C. Two pairs of sloping voltage plateaus are evident at about 2.3 and 0.5 V vs. Na^+/Na which mark the redox reactions of Ti present in the cycling process. These voltage profiles are in agreement with the CV analysis (Figure 3a, b).

Figure 4(a,b) demonstrates significantly higher sodiation and desodiation capacities for NTP-RT compared to NTP as well as for NTP/C-RT compared to NTP/C. NTP has a theoretical capacity of 133 mAh/g. While the theoretical capacity of rutile is 336 mAh/g.^[33] Sodiation/ desodiation capacities of NTP measurements here are lower compared to the theoretical capacity value. On the other hand, very high capacities beyond the theoretical capacity of NTP are found for the carbon-coated samples. Moreover, the rutile coating has also a significant, positive influence on the gravimetric capacities, which can be attributed to the higher theoretical capacity of rutile. Our results, therefore, clearly show that carbon and rutile coating enhances the intrinsic electrical conductivity, and results in higher sodiation/desodiation capacities. Sodiation as well as desodiation capacities decrease with increasing cycle numbers. As a result, the capacity fades during cycling of the battery, which can significantly shorten the battery lifetime. The cycle stability is, among other factors, dependent on a stable crystal framework and a good particle to particle electrical contact.^[34]

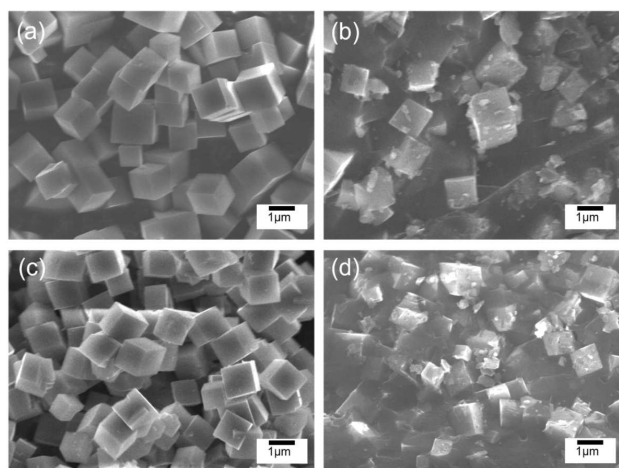


Figure 2. SEM images of a) NTP, b) NTP/C, c) NTP-RT and d) NTP/C-RT, showing the NC morphology.

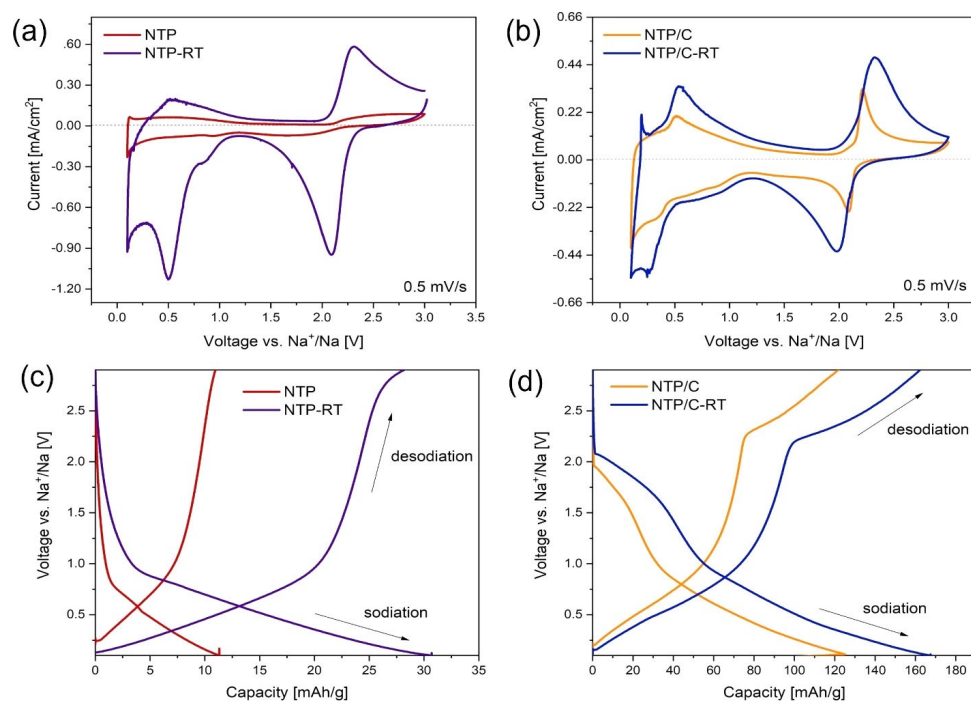


Figure 3. Cyclic voltammograms of a) NTP and NTP-RT, b) NTP/C and NTP/C-RT, all recorded at a scan rate of 0.5 mV/s. Rate performance voltammogram of c) NTP versus NTP-RT and d) NTP/C versus NTP/C-RT.

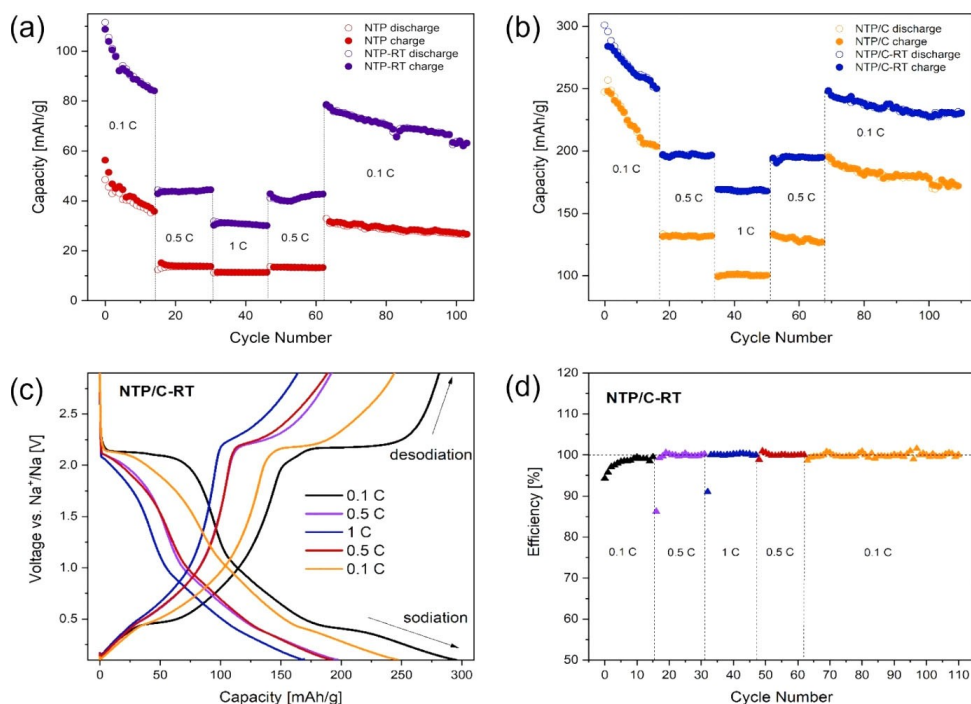


Figure 4. Sodiation/desodiation capacities at increasing cycle numbers for a) NTP and NTP-RT, b) NTP/C and NTP/C-RT. c) Sodiation/desodiation curves at different C-rates and d) Coulombic efficiencies for NTP/C-RT.

It can be concluded that the carbon-coated samples possess better electrical conductivity, since the highest reversible capacities are achieved with NTP/C-RT. Maximum sodiation/desodiation rates, of 56, 120, 248 and 301 mAh/g were found for NTP, NTP-RT, NTP/C and NTP/C-RT, respectively. The highest

rate capabilities of 301 mAh/g were found for NTP/C-RT at a C-rate of 0.1. Distinctively higher rate capabilities could be achieved for the rutile coated samples over non-coated samples, corroborating that rutile coating improves the specific

capacity and surface stability. Additional carbon coating can further enhance the rate capabilities.

The enhanced electrical conductivity has been confirmed with impedance measurements (see Supporting Information Figure S3). Ohmic and charge transfer resistance values are higher for NTP compared to NTP/C. This increasing resistance trend can also be seen between NTP-RT and NTP.

For all samples, a significant decrease in capacity can be observed during the first 15 cycles at 0.1 C. For the following 45 cycles reversible capacities could be obtained. The capacity retention is calculated after 100 cycles and delivers values of 49, 52, 69 and 77% for NTP, NTP-RT, NTP/C and NTP/C-RT, respectively. This indicates a significantly higher cycling stability for carbon-coated samples. The low-capacity retention is not fully understood by now. It could, however, be a sign of dissolution of active material from the electrode and consequently missing electrical contact, solid electrolyte interface (SEI) formation or the result of irreversible side reactions. In all samples a steep capacity drop can be seen in the first 15 cycles at 0.1 C, which is the main contribution for the calculated decrease in capacity retention. This steep initial capacity drop is usually attributed to SEI formation.^[35] For the next 85 cycles the capacity remains almost stable. The poor cycling stability of NTP and NTP-RT can also be induced by a self-aggregation of the active material particles, which leads to poor electrical contact.^[20] Consequently, carbon coating can prevent self-aggregation, which offers a proper network for electron transport. NTP/C-RT shows the highest capacity retention, therefore rutile coating can further enhance the cycling stability.

Figure 4(d) shows the Coulombic efficiencies (CE) for NTP/C-RT. Based on the high CE values, low internal resistance of the cell can be assumed. CE for NTP, NTP/C and NTP-RT are shown in the Supporting Information Figure S2(a–c).

Conclusions

Stable anode materials are currently the limiting factor hampering the development of high-performance SIBs. This is being verified, considering the fact that the investigated NTP anode is electrically limited by conductivity and kinetically limited to slow scan rates. Therefore, enhancement strategies, like the one developed in this work for the anode materials are essential.

Carbon and simultaneous rutile coating is an easy and feasible enhancement strategy, demonstrating a significant improvement on the materials performance. Carbon-coated NTP is already a promising candidate as anode material for SIBs.^[26,36] Rutile coating further contributes to the enhancement on the NTP anode material, to optimize its performance and overcome its limiting properties.

SEM images show highly symmetrical, uniform NTP NCs that were synthesized by a simple and reproducible solvothermal method. XRD measurements prove the high purity for NTP.

For NTP, carbon coating results in a significant electrochemical improvement, which leads to the conclusion that pure NTP is limited by its low intrinsic electrical conductivity. NTP shows higher reversibility at slow scan rates and its perform-

ance in Na-ion batteries is consequently kinetically limited by a slow Na-ion diffusion and its low conductivity.

NTP-RT shows improved electrochemical performance compared to pristine NTP, meaning that rutile enhances the electrical conductivity and/or the Na-ion diffusion. This could be confirmed with impedance measurements.

The presence of rutile confirmed by Raman spectroscopy, XRD and XPS measurements. Best results are achieved using NTP/C-RT, with an initial sodiation capacity of 301 mAh/g. Well-defined sodiation and desodiation plateaus and a capacity retention of 77% prove a high cycling stability. In general, CEs close to 100% could be reached for all NTP samples.

Particularly, the advantages of SIBs, like low-cost, environmental friendliness, high material abundance and high safety, make them an essential part of next generation batteries. The large amount of research devoted to the field of SIBs in the past few years and to date, fuels the hope for scientific breakthroughs for aqueous SIBs in the near future. The experiments conducted in this work identify some key limiting properties for the NTP anode and reveal an effective approach for its improvement. Furthermore, the simple synthesis methods performed for NTP could prove that a large-scale production is easily feasible.

Supporting Information

The authors have cited additional references within the Supporting Information.^[37–39]

Acknowledgements

We gratefully acknowledge the support of the Austrian Science Fund (FWF) within the FWF project P34233 and P35510, as well as the support of the Austrian Research Promotion Agency (FFG) within the FFG project 877095.

Conflict of Interests

The authors declare no conflict of interest.

Data Availability Statement

The data that support the findings of this study are available from the corresponding author upon reasonable request.

Keywords: sodium Ion Batteries · electrochemistry · anode material · NTP · sodium titanium phosphate

[1] J. Lin, X. Zhang, E. Fan, R. Chen, F. Wu, L. Li, *Energy Environ. Sci.* **2023**, *16*, 745–791.

[2] H. Kim, J. Hong, K.-Y. Park, H. Kim, S.-W. Kim, K. Kang, *Chem. Rev.* **2014**, *114*, 11788–11827.

- [3] N. Tapia-Ruiz, A. R. Armstrong, H. Alptekin, M. A. Amores, H. Au, J. Barker, R. Boston, W. R. Brant, J. M. Brittain, Y. Chen, M. Chhowalla, Y.-S. Choi, S. I. R. Costa, M. Crespo Ribadeneyra, S. A. Cussen, E. J. Cussen, W. I. F. David, A. V. Desai, S. A. M. Dickson, E. I. Eweka, J. D. Forero-Saboya, C. P. Grey, J. M. Griffin, P. Gross, X. Hua, J. T. S. Irvine, P. Johansson, M. O. Jones, M. Karlsmo, E. Kendrick, E. Kim, O. V. Kolosov, Z. Li, S. F. L. Mertens, R. Mogensen, L. Monconduit, R. E. Morris, A. J. Naylor, S. Nikman, C. A. O'Keefe, D. M. C. Ould, R. G. Palgrave, P. Poizot, A. Ponrouch, S. Renault, E. M. Reynolds, A. Rudola, R. Sayers, D. O. Scanlon, S. Sen, V. R. Seymour, B. Silván, M. T. Sougrati, L. Stievano, G. S. Stone, C. I. Thomas, M.-M. Titirici, J. Tong, T. J. Wood, D. S. Wright, R. Younesi, *J. Phys. Energy* **2021**, *3*, 031503.
- [4] H. Zhang, X. Liu, H. Li, I. Hasa, S. Passerini, *Angew. Chem. Int. Ed. Engl.* **2021**, *60*, 598–616.
- [5] H. Moriwake, A. Kuwabara, C. A. J. Fisher, Y. Ikuhara, *RSC Adv.* **2017**, *7*, 36550–36554.
- [6] M. D. Slater, D. Kim, E. Lee, C. S. Johnson, *Adv. Funct. Mater.* **2013**, *23*, 947–958.
- [7] S. Liebl, D. Werner, D. H. Apaydin, D. Wielend, K. Geistlinger, E. Portenkirchner, *Chemistry* **2020**, *26*, 17559–17566.
- [8] D. Werner, D. H. Apaydin, E. Portenkirchner, *Batteries & Supercaps* **2018**, *1*, 160–168.
- [9] D. Werner, C. Griesser, D. Stock, U. J. Griesser, J. Kunze-Liebhäuser, E. Portenkirchner, *ACS Appl. Energ. Mater.* **2020**, *3*, 3477–3487.
- [10] L. Szabados, D. Winkler, D. Stock, T. Alexander, T. Lörting, J. Kunze-Liebhäuser, E. Portenkirchner, *Adv. Energy Sustain. Res.* **2022**, *3*, 2200104.
- [11] J.-Y. Hwang, S.-T. Myung, Y.-K. Sun, *Chem. Soc. Rev.* **2017**, *46*, 3529–3614.
- [12] N. Ortiz-Vitoriano, N. E. Drewett, E. Gonzalo, T. Rojo, *Energy Environ. Sci.* **2017**, *10*, 1051–1074.
- [13] Y. Fang, L. Xiao, Z. Chen, X. Ai, Y. Cao, H. Yang, *Electrochem. Energy Rev.* **2018**, *1*, 294–323.
- [14] B. Zhao, Q. Wang, S. Zhang, C. Deng, *J. Mater. Chem. A* **2015**, *3*, 12089–12096.
- [15] D. Winkler, T. Stüwe, D. Werner, C. Griesser, C. Thurner, D. Stock, J. Kunze-Liebhäuser, E. Portenkirchner, *Electrochem. Sci. Adv.* **2022**, e2200012.
- [16] H. Gao, J. B. Goodenough, *Angew. Chem.* **2016**, *128*, 12960–12964.
- [17] E. Portenkirchner, S. Rommel, L. Szabados, C. Griesser, D. Werner, D. Stock, J. Kunze-Liebhäuser, *NanoSelect* **2021**, *2*, 1533–1543.
- [18] E. Portenkirchner, D. Werner, S. Liebl, D. Stock, A. Auer, J. Kunze-Liebhäuser, *ACS Appl. Energ. Mater.* **2018**, *1*, 6646–6653.
- [19] G. Pang, P. Nie, C. Yuan, L. Shen, X. Zhang, H. Li, C. Zhang, *J. Mater. Chem. A* **2014**, *2*, 20659–20666.
- [20] C. Wu, P. Kopold, Y.-L. Ding, P. A. van Aken, J. Maier, Y. Yu, *ACS Nano* **2015**, *9*, 6610–6618.
- [21] G. Plečkaitytė, M. Petrulėvičienė, L. Staišiūnas, D. Tediashvili, J. Pilipavičius, J. Juodkazytė, L. Vilčiauskas, *J. Mater. Chem. A* **2021**, *9*, 12670–12683.
- [22] Z.-G. Liu, R. Du, X.-X. He, J.-C. Wang, Y. Qiao, L. Li, S.-L. Chou, *ChemSusChem* **2021**, *14*, 3724–3743.
- [23] L. Wang, Z. Huang, B. Wang, G. Liu, M. Cheng, Y. Yuan, H. Luo, T. Gao, D. Wang, R. Shahbazian-Yassar, *ACS Appl. Mater. Interfaces* **2019**, *11*, 10663–10671.
- [24] D. Wang, Q. Liu, C. Chen, M. Li, X. Meng, X. Bie, Y. Wei, Y. Huang, F. Du, C. Wang et al., *ACS Appl. Mater. Interfaces* **2016**, *8*, 2238–2246.
- [25] Z. Wang, J. Liang, K. Fan, X. Liu, C. Wang, J. Ma, *Front. Chem.* **2018**, *6*, 396.
- [26] M. Wu, W. Ni, J. Hu, J. Ma, *Nano-Micro Lett.* **2019**, *11*, 1–36.
- [27] W. Wu, J. Yan, A. Wise, A. Rutt, J. F. Whitacre, *J. Electrochem. Soc.* **2014**, *161*, A561–A567.
- [28] J. Li, J. Fleetwood, W. B. Hawley, W. Kays, *Chem. Rev.* **2022**, *122*, 903–956.
- [29] F. Yu, L. Du, G. Zhang, F. Su, W. Wang, S. Sun, *Adv. Funct. Mater.* **2020**, *30*, 1906890.
- [30] L.-C. Zhang, Y. Zhou, Y.-Q. Li, W.-L. Ma, P. Wu, X.-S. Zhu, S.-H. Wei, Y.-M. Zhou, *J. Solid State Chem.* **2022**, *310*, 123036.
- [31] J.-B. Wu, M.-L. Lin, X. Cong, H.-N. Liu, P.-H. Tan, *Chem. Soc. Rev.* **2018**, *47*, 1822–1873.
- [32] W. Gao, Y. Wan, Y. Dou, D. Zhao, *Adv. Energy Mater.* **2011**, *1*, 115–123.
- [33] B. Zhao, R. Cai, S. Jiang, Y. Sha, Z. Shao, *Electrochim. Acta* **2012**, *85*, 636–643.
- [34] X. Li, X. Zhu, J. Liang, Z. Hou, Y. Wang, N. Lin, Y. Zhu, Y. Qian, *J. Electrochem. Soc.* **2014**, *161*, A1181–A1187.
- [35] J. Yang, H. Wang, P. Hu, J. Qi, L. Guo, L. Wang, *Small* **2015**, *11*, 3744–3749.
- [36] G. Yang, H. Song, M. Wu, C. Wang, *J. Mater. Chem. A* **2015**, *3*, 18718–18726.
- [37] T. Mazza, E. Barborini, P. Piseri, P. Milani, D. Cattaneo, A. Li Bassi, C. E. Bottani, C. Ducati, *Phys. Rev. B* **2007**, *75*, 045418.
- [38] S. Challagulla, K. Tarafder, R. Ganesan, S. Roy, *Sci. Rep.* **2017**, *7*, 8783.
- [39] G. Xu, Z. Li, X. Wei, L. Yang, P. K. Chu, *Electrochim. Acta* **2017**, *254*, 328–336.

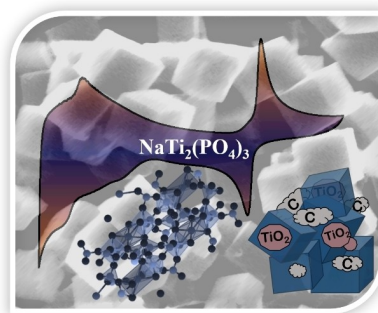
Manuscript received: May 31, 2023

Revised manuscript received: July 25, 2023

Version of record online: ■■, ■■

RESEARCH ARTICLE

Stable anode: NTP is considered as a promising anode material for sodium-ion batteries in aqueous and non-aqueous electrolyte environments. In this work, an approach which combines the synthesis of NTP nanocubes, rutile TiO_2 coating and carbon coating, was chosen. Our results demonstrate superior capacities than reported elsewhere.



*T. Stüwe, D. Werner, D. Stock, C. W. Thurner, A. Thöny, C. Griebner, Dr. T. Loerting, Dr. E. Portenkirchner**

1 – 7

Enhanced Electrochemical Performance of NTP/C with Rutile TiO_2 Coating, as Anode Material for Sodium-Ion Batteries

